Raman scattering study of the $Fe_{1-x}Co_xSb_2$ and $Fe_{1-x}Cr_xSb_2$ $(0 \leq x \leq 1)$ single crystals

N. Lazarević and Z. V. Popović
Center for Solid State Physics and New Materials, Institute of Physics, Pregrevica 118, 11080 Belgrade, Serbia

Rongwei Hu
Department of Condensed Matter Physics and Materials Science, Brookhaven National Laboratory, Upton, New York 11973-5000, USA and Department of Physics, Brown University, Providence, Rhode Island 02912, USA

C. Petrovic
Department of Condensed Matter Physics and Materials Science, Brookhaven National Laboratory, Upton, New York 11973-5000, USA
(Received 15 April 2009; revised manuscript received 15 June 2009; published 6 July 2009)

Polarized Raman scattering spectra of the $Fe_{1-x}Co_xSb_2$ and $Fe_{1-x}Cr_xSb_2$ $(0 \leq x \leq 1)$ single crystals are measured at room temperature in the 80–200 cm^{-1} wavenumber range. All six Raman-active modes, predicted by factor-group analysis, are experimentally observed and assigned. We also analyzed energy and linewidth changes for all six Raman-active modes caused by doping.

DOI: 10.1103/PhysRevB.80.014302 PACS number(s): 78.30.Hv, 72.20.−i, 75.20.−g, 73.63.−b

I. INTRODUCTION

Theoretical description of Ce and Fe containing strongly correlated insulators has been a long-standing issue.[1] The heart of the problem is localized to an itinerant crossover and a hybridization gap involving $4f$ or $3d$ electrons.[2,3] $FeSb_2$ is a narrow-gap semiconductor which recently attracted a lot of attention because of its unusual magnetic properties (paramagnetic to diamagnetic crossover at around 100 K),[4] thermoelectric properties (colossal Seebeck coefficient S at 10 K and the largest power factor $S^2\sigma$ ever reported),[5] and transport properties (a metal to semiconductor transition at around 40 K).[6]

The optical properties of $FeSb_2$ were studied by Perucchi *et al.*[7] by measuring the reflectivity spectra in the wide spectral range (from far infrared up to UV). The Raman scattering measurements in $FeSb_2$ were analyzed, to the best of our knowledge, only in Refs. 8 and 9. Lutz and Müller[8] observed two Raman-active modes at about 175 and 154 cm^{-1} by unpolarized Raman scattering measurements of hot-pressed samples and assigned as modes of the A_g symmetry. Contrary to them, Racu *et al.*,[9] using polarized Raman scattering measurements on $FeSb_2$ single crystals, observed three Raman modes at about 150, 157, and 180 cm^{-1} and assigned them as the B_{1g}, A_g, and B_{1g} symmetry modes, respectively. No Raman scattering study of doped $FeSb_2$ has been published so far.

In order to resolve above mentioned controversy, we have measured the polarized Raman scattering spectra of differently oriented single-crystal samples of pure and electron-doped (Co) and hole-doped (Cr) $FeSb_2$. We have observed and assigned all six Raman-active modes predicted by symmetry. We have also analyzed both a Raman-mode energy and a broadening change caused by doping with Co and Cr.

II. EXPERIMENT

Single crystals of $FeSb_2$, $Fe_{1-x}Co_xSb_2$, and $Fe_{1-x}Cr_xSb_2$ $(0<x\leq 1)$ were grown using the high-temperature flux method, which is described in detail in Refs. 10 and 11. Sample structure and composition were determined by analyzing the x-ray-diffraction data of $Fe(Co,Cr)Sb_2$ single crystals collected using a Bruker SMART 1000 diffractometer with charge-coupled-device detector and Mo $K\alpha$ radiation.[12,13] The stoichiometries were determined by an energy dispersive JEOL JSM-6500 scanning electron microscopy microprobe. Analysis of several nominal $x=0.25$ samples showed that the uncertainty in Co and Cr concentrations among samples grown from different batches was $\Delta x=0.04$. Crystals were oriented using a Laue camera and polished into rectangular bars along specific crystalline axes.

The Raman scattering measurements were performed using a Jobin Yvon T64000 Raman system in micro-Raman configuration. The 514.5 nm line of an Ar^+-ion laser was used as an excitation source. Laser power at the sample was about 1 mW. All the measurements were performed in air at room temperature. In order to obtain all Raman-tensor components, we have used differently oriented samples in different polarization configurations of incident and scattered light.

III. RESULTS AND DISCUSSION

$FeSb_2$ crystallizes in the orthorhombic marcasite-type structure. The basic structural unit is built of Fe ions surrounded by deformed Sb octahedra. These units form edge-sharing chains along the c axis, see Fig. 1. The space group is centrosymmetric $Pnnm$ (D_{2h}^{12}), with two formula units $(Z=2)$ per unit cell.[14] Factor-group analysis yields a normal-mode distribution at the center of the Brillouin zone,

$$\Gamma_{FeSb_2} = 2A_g(aa,bb,cc) + 2B_{1g}(ab) + B_{2g}(ac) + B_{3g}(bc) + 2A_u(silent) + 2B_{1u}(\mathbf{E}\parallel\mathbf{c}) + 4B_{2u}(\mathbf{E}\parallel\mathbf{b}) + 4B_{3u}(\mathbf{E}\parallel\mathbf{a}).$$

According to this representation, in the Raman scattering experiment one can expect a total of 6 Raman-active modes.

For Raman scattering measurements we mostly used the $(10\bar{1})$ plane. Selection rules for parallel and crossed polariza-

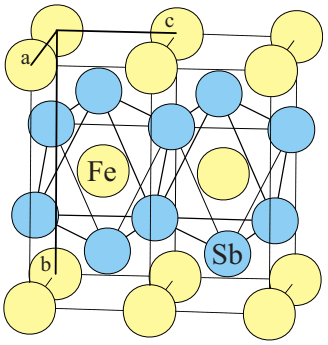

FIG. 1. (Color online) Schematic representation of the $FeSb_2$ crystal structure.

tion from the $(10\bar{1})$ plane are summarized in Table I. The (yy) configuration denotes polarizer and analyzer polarization direction parallel to the b axis of $FeSb_2$ crystal. In this case, only the A_g symmetry modes can be observed. The $(x'x')$ configuration denotes polarization in the (ac) plane along the $x'=[101]$ direction (perpendicular to the b axis). In this case both the A_g and B_{2g} symmetry modes can be observed. For a crossed $(x'y)$ polarization configuration the B_{1g} and B_{3g} modes appear.

The room-temperature-polarized Raman spectra of pure $FeSb_2$, 25%-Cr-doped, and 25%-Co-doped $FeSb_2$ single crystals in all three principal polarizations are presented in Fig. 2. The notations are those from Table I. For pure $FeSb_2$, in both the (yy) and $(x'x')$ polarization configurations, we have observed one structure at about 151 cm^{-1}, which shows a slight asymmetry toward higher wave numbers. This structure is well fitted with two Lorentzian profile lines, as shown in Fig. 2. The existence of a two-peak structure becomes more obvious by doping the $FeSb_2$ with Co, see Fig. 2. Thus,

TABLE I. Raman tensors for orthorhombic crystal structure and selection rules for $(10\bar{1})$ plane of $FeSb_2$ orthorhombic crystal symmetry.

Raman tensors	
$A_g=\begin{pmatrix} a & 0 & 0 \\ 0 & b & 0 \\ 0 & 0 & c \end{pmatrix}$	$B_{1g}=\begin{pmatrix} 0 & d & 0 \\ d & 0 & 0 \\ 0 & 0 & 0 \end{pmatrix}$
$B_{2g}=\begin{pmatrix} 0 & 0 & e \\ 0 & 0 & 0 \\ e & 0 & 0 \end{pmatrix}$	$B_{3g}=\begin{pmatrix} 0 & 0 & 0 \\ 0 & 0 & f \\ 0 & f & 0 \end{pmatrix}$
Symmetry	Polarization configuration
A_g	$(x'x'),(yy)$
B_{1g}	$(x'y)$
B_{2g}	$(x'x')$
B_{3g}	$(x'y)$
$y=[010]$	$x'=\frac{1}{\sqrt{2}}[101]$

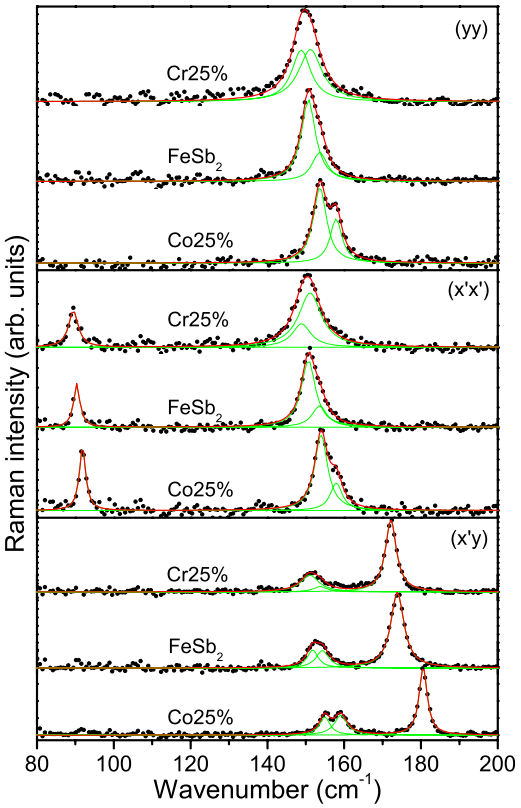

FIG. 2. (Color online) The room-temperature-polarized Raman spectra of pure $FeSb_2$, 25%-Cr-doped, and 25%-Co-doped single crystals in three polarization configurations. The notation in the parentheses indicates the polarization directions of the incident and scattered light, respectively.

we concluded that Raman modes at about 150.7 and 153.6 cm^{-1} are of the A_g symmetry. For the $(x'x')$ polarization configuration, one additional mode appears at about 90.4 cm^{-1}, which is assigned, according to the selection rules given in Table I, as the B_{2g} symmetry mode. For crossed polarization $(x'y)$, we easily distinguished three Raman modes at about 151.7, 154.3, and 173.9 cm^{-1}, which can be of the B_{1g} or B_{3g} symmetry. Because the B_{3g} mode has the lowest energy in comparison to the B_{1g} modes in all marcasite-type iron chalcogenides,[8] we assigned the 151.7 cm^{-1} mode as the B_{3g} symmetry one. Two other modes observed for crossed polarization at about 154.3 and 173.9 cm^{-1} are the B_{1g} symmetry ones. In addition, the appearance of B_{1g} symmetry modes in $FeSb_2$ at energies higher than A_g symmetry is fully in agreement with Raman spectra of other isostructural marcasite-type compounds.[8] Comparing our work with previously published results (Table II), we found some disagreement which apparently is due to the incorrect mode assignment based on unpolarized measurements in Ref. 8 and the use of the (110) plane of the $FeSb_2$ sample in Raman scattering measurements[9] from which both A_g and B_{1g} modes can be observed.

Since Fe atoms are located in the center of inversion of the *Pnnm* space group, they do not contribute to the Raman scattering process, i.e., all six Raman modes in $FeSb_2$ represent vibrations of Sb atoms. The highest-energy A_g and B_{1g} modes originate from the bond-stretching vibrations of

TABLE II. Raman-mode wave numbers (in cm^{-1}) of $FeSb_2$ single crystal at room temperature.

Symmetry	This work	Reference 8	Reference 9
B_{1g}	173.9		180
B_{1g}	154.3		150
A_g	153.6	175	157
B_{3g}	151.7		
A_g	150.7	154	
B_{2g}	90.4		

$FeSb_6$ octahedra and all other modes should be rotational ones.[8] Appearance of two A_g symmetry modes at energies very close to each other means that there is a strong mixing of stretching and rotational vibrations of the A_g symmetry modes.

Physical properties of $FeSb_2$ change dramatically with Co and Cr doping.[5,12,13,15] The semiconducting ground state of $FeSb_2$ evolves into a metallic at $x=0.1$ in $Fe_{1-x}Co_xSb_2$. Further increase in Co concentration induces weak ferromagnetism for $0.2 \leq x \leq 0.54$. Beyond $x=0.5$, there is a structural transformation from orthorhombic *Pnnm* to the pseudomarcasite monoclinic $P2_1/c$ structure of $CoSb_2$ with a small monoclinic angle $\beta=90.4°$ and the reestablishing of the anisotropic semiconducting ground state for $0.5<x<1$.[12] Since $CrSb_2$ crystallizes in an orthorhombic marcasite *Pnnm* structure, the complete substitution of Fe ions with Cr ions is possible. With the increase of x in $Fe_{1-x}Cr_xSb_2$ sample, the paramagnetic ground state evolves toward an antiferromagnetic one. The c-axis transport is metallic for $0 \leq x \leq 0.25$.[15] All these effects have no influence on the Raman spectra of $Fe(Co,Cr)Sb_2$ at room temperature except for the orthorhombic-to-monoclinic structural phase transition in the Co-doped system for $x>0.5$ (Fig. 3).

Raman-modes frequency shift for $Fe_{1-x}Co_xSb_2$ and $Fe_{1-x}Cr_xSb_2$ as a function of Co and Cr concentrations are shown in Fig. 3. For $Fe_{1-x}Co_xSb_2$, it can be seen that all Raman modes are shifted toward higher energies, but for $Fe_{1-x}Cr_xSb_2$ they are shifted toward lower energies. The main reason for the mode-energy shift is that the lattice parameters change by dopant concentration increase. The effect of mass change is excluded because Fe (Co, Cr) atom is in the center of inversion and does not contribute to the Raman scattering spectra in a direct way. Cobalt substitution leads to the unit-cell contraction, i.e., unit-cell volume (V) decreases about 5% for $x=0.4$.[14] We can make an approximate estimate for the change in the phonon frequency of the bond-stretching modes. It is known[16] that scaling of the phonon frequency for the bond-stretching mode is R^{-3} where R is the bond length. If we take that change in R^{-3} is proportional to the volume change V^{-1}, we can expect the phonon-frequency change for bond-stretching A_g and B_{1g} modes to be inversely proportional to the volume change (i.e., of about 5% for $x=0.4$), which is in complete agreement with experimental findings, Fig. 3. By further increase in the Co concentration ($x>0.5$), the orthorhombic unit cell of $FeSb_2$, with the *Pnnm* space-group symmetry and $Z=2$, transforms into a monoclinic unit cell of $P2_1/c$ space-group symmetry and $Z=4$. In this case the total number of Raman modes increases from 6 to 18 ($9A_g+9B_g$). The appearance of new Raman modes can be already seen for $x=0.6$ sample, whereas the Raman spectrum of $FeCo_2$ ($x=1$) differs completely from $FeSb_2$, as it can be observed in the inset at the left panel of Fig. 3.

Chromium substitution results in the unit-cell expansion of about 0.8% for $x=0.4$.[15] Therefore we can expect a slight mode-frequency softening by doping, as it is shown at the right panel of Fig. 3. Doping generally induces structural disorder, which increases phonon-mode broadening. Such effect is illustrated in the inset at right panel of Fig. 3 for the $Fe_{1-x}Cr_xSb_2$ case.

IV. CONCLUSION

We have studied $Fe_{1-x}Co_xSb_2$ and $Fe_{1-x}Cr_xSb_2$ samples in a wide range of dopant concentrations using Raman scatter-

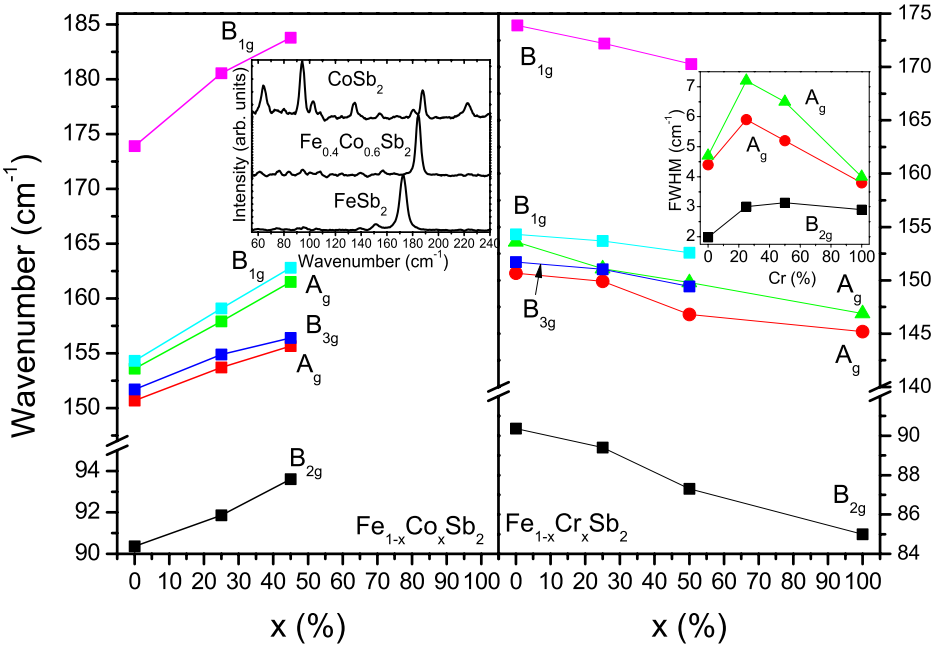

FIG. 3. (Color online) Raman-mode frequency shifts as a function of dopant concentrations x. Inset at the left panel: Unpolarized Raman spectra of $Fe_{1-x}Co_xSb_2$ for $x=0$; 0.6, and 1. Inset at the right panel: full width at half maximum of the A_g and B_{2g} modes at room temperature as a function of Cr concentration x.

ing spectroscopy. All six Raman-active modes, predicted by the factor-group analysis of the *Pnnm* symmetry of $FeSb_2$, are observed and assigned. After analyzing Raman-mode energy shifts as a function of Co and Cr concentration, we conclude that change in the unit-cell volume has major contribution in the mode shifting. The broadening of the Raman lines with the increase in dopant concentration x is a consequence of the increase in structural disorder.

ACKNOWLEDGMENTS

We thank Myron Strongin for help with the paper. This work was supported by the Serbian Ministry of Science and Technological Development under Project No. 141047. Part of this work was carried out at the Brookhaven National Laboratory which is operated for the Office of Basic Energy Sciences, U.S. Department of Energy by Brookhaven Science Associates (Grant No. DE-Ac02-98CH10886).

[1] Z. Fisk and G. Aeppli, Comments Condens. Matter Phys. **16**, 155 (1992).
[2] V. I. Anisimov, R. Hlubina, M. A. Korotin, V. V. Mazurenko, T. M. Rice, A. O. Shorikov, and M. Sigrist, Phys. Rev. Lett. **89**, 257203 (2002).
[3] M. Jaime, R. Movshovich, G. R. Stewart, W. P. Beyermann, M. G. Berisso, M. F. Hundley, P. C. Canfield, and J. L. Sarrao, Nature (London) **405**, 160 (2000).
[4] C. Petrovic, J. W. Kim, S. L. Bud'ko, A. I. Goldman, P. C. Canfield, W. Choe, and G. J. Miller, Phys. Rev. B **67**, 155205 (2003).
[5] A. Bentien, S. Johnsen, G. K. H. Madsen, B. B. Iversen, and F. Steglich, EPL **80**, 39901 (2007).
[6] R. Hu, V. F. Mitrović, and C. Petrovic, Appl. Phys. Lett. **92**, 182108 (2008).
[7] A. Perucchi, L. Degiorgi, Rongwei Hu, C. Petrovic, and V. F. Mitrović, Eur. Phys. J. B **54**, 175 (2006).
[8] H. D. Lutz and B. Müller, Phys. Chem. Miner. **18**, 265 (1991).
[9] A.-M. Racu, D. Menzel, J. Schoenes, M. Marutzky, S. Johnsen, and B. B. Iversen, J. Appl. Phys. **103**, 07C912 (2008).
[10] Z. Fisk and J. P. Remeika, in *Handbook on the Physics and Chemistry of Rare Earths*, edited by K. A. Gschneider and J. Eyring (Elsevier, Amsterdam, 1989), Vol. 12.
[11] P. C. Canfield and Z. Fisk, Philos. Mag. B **65**, 1117 (1992).
[12] Rongwei Hu, V. F. Mitrović, and C. Petrovic, Phys. Rev. B **74**, 195130 (2006).
[13] R. Hu, R. P. Hermann, F. Grandjean, Y. Lee, J. B. Warren, V. F. Mitrovic, and C. Petrovic, Phys. Rev. B **76**, 224422 (2007).
[14] C. Petrovic, Y. Lee, T. Vogt, N. Dj. Lazarov, S. L. Bud'ko, and P. C. Canfield, Phys. Rev. B **72**, 045103 (2005).
[15] Rongwei Hu, V. F. Mitrović, and C. Petrovic, Phys. Rev. B **76**, 115105 (2007).
[16] Z. V. Popović, V. Stergiou, Y. S. Raptis, M. J. Konstantinović, M. Isobe, Y. Ueda, and V. V. Moshchalkov, J. Phys.: Condens. Matter **14**, L583 (2002).